ROYAL SOCIETY
OF CHEMISTRY

## PAPER

Check for updates

# Enhancing the graphitization ability of corn-cob-derived lignin by coupling stabilization and hot-pressing

Xiuxia Zhang, [ID] [a] Xiao Han, [ID] [a] Jing Liu, [b] Fangxiao Feng, [a] Chen Liang, [c] Linghong Yin*[a] and Wangda Qu*[a]

Lignin's non-graphitizable behavior is one of the key issues that impede its wide applications as carbon materials. Following our invention of using hot-pressing to facilitate lignin graphitization, this work focuses on converting an enzymatic herbaceous lignin which is less reactive and inherently contains long side-chains, and therefore follows a different pathway to graphitize compared with lignin from wood. This work presents more systematic investigation into the conversion of raw lignin to graphitizable carbon with better graphitic structure by stabilization and hot-pressing. Results show that lignin requires a suitable stabilization temperature to enhance its compressibility and high-pressure resistance, enabling its transformation into graphitizable structures. This work gives details in the characterization results of lignin, tracing its transformation from the raw state to carbonized samples, and elucidating the structural evolution during hot-pressing and carbonization. This study further identifies the optimal stabilization temperature as 320 °C, along with a hot-pressing temperature of 290 °C and a pressure of 18 tons at a low-carbonization temperature of 1000 °C. The carbonized LSHC-320-290-18 sample exhibits a significantly higher $2\theta$ value of 25.26° at the (002) diffraction peak in the XRD spectrum.

## 1 Introduction

Developing highly graphitic carbon materials from lignin has emerged as a key route to expand lignin valorization. However, lignin-derived carbons are typically amorphous owing to the irregular and complex structure.[1,2] Currently, the main strategies to enhance graphitic ordering mainly include: (i) ultrahigh-temperature pyrolysis (2000–3000 °C),[3] (ii) catalytic graphitization,[4] and (iii) templating approaches.[5] Although high-temperature treatments can effectively promote sp[2] carbon reorganization, the requirement for temperatures above 2000 °C leads to excessive energy consumption and high operational costs, limiting industrial feasibility.[6] While catalytic graphitization can reduce graphitization temperatures and improve energy efficiency, issues related to catalyst selection, recyclability, and contamination risks.[7] Template-assisted methods can enhance lignin's graphitic structure, but the structural heterogeneity, performance inconsistency, and the complexity of template synthesis and removal constrain their large-scale

application.[8] Our previous work has demonstrated that hot-pressing technology considerably enhances the graphitization potential of lignin by facilitating methoxyl group decomposition and triggering intermolecular linkage formation.[9] These structural transformations create favorable thermodynamic conditions for aromatization during carbonization, thereby yielding carbonaceous materials with enhanced graphitic crystallinity.[9] Compared with traditional approaches, hot-pressing provides a controllable and energy-efficient pathway for producing lignin-derived graphitic carbons, demonstrating significant promise for scalable fabrication of high-performance carbon materials.

Corn-cobs exhibit much shorter growth cycles and faster growth rates than woody plants. During the rapid cell division and elongation phases, lignin deposition in cell walls occurs under time-constrained conditions, leading to the preferential formation of highly branched macromolecular structures.[10] These structures are characterized by extended polymeric chains formed through accelerated biosynthetic processes. Lignin extraction from corn-cobs is commonly achieved *via* hot alkaline treatment,[11] organic solvent extraction,[12] enzymatic hydrolysis,[13] high-temperature pyrolysis,[13] and mechanical pulverization.[14] Among these methods, enzymatic hydrolysis lignin (EHL) is mainly produced as a byproduct in biorefineries during cellulose ethanol, xylose, and furfural production, representing a major form of agricultural residue. The mild

*[a]Laboratory of Lignin-based Materials, College of Life Sciences, Qingdao Agricultural University, Qingdao 266109, China. E-mail: wqu@qau.edu.cn; lhyin@qau.edu.cn*
*[b]College of New Materials and New Energies, Shenzhen Technology University, Shenzhen, 518116, China*
*[c]College of Chemistry and Pharmaceutical Sciences, Qingdao Agricultural University, Qingdao 266109, China*

reaction conditions of enzymatic hydrolysis preserve the native lignin framework and retain abundant oxygen-containing functional groups, making EHL particularly attractive for high-value utilization.[15] However, herbaceous EHL exhibits long-branched molecular configurations that generate significant steric hindrance,[16] impeding close molecular packing and the ordered arrangement required for the formation of well-defined graphitic layers.[17,19] So far, the research on graphitization methods of this type of lignin remains limited. The hot-pressing process offers a potential solution by mitigating the intrinsic steric constraints inherent in EHL.[18] When pressure is applied, the long branches are forced to rearrange, enabling more effective molecular alignment. As a result, this rearrangement provides a favorable foundation for subsequent aromatization and carbonization reactions, thereby facilitating graphitization.[20] In addition, during hot-pressing, the temperature not only provides energy to the lignin molecules, but also enhances molecular mobility, allowing lignin chains to move, rotate, and interact within a confined range.[21] These dynamic interactions promote bond recombination, which drives structural reorganization toward graphitic ordering. To achieve optimal graphitization, the stabilization temperature, hot-pressing temperature, and pressure must be carefully tuned. Nonetheless, the specific effects of these parameters on producing highly graphitized carbon from EHL derived from corn-cobs through hot-pressing remain unknown.

This study systematically investigates the graphitization mechanisms of corncob-derived enzymatic hydrolysis lignin (EHL) by coordinately tuning the stabilization temperature, hot-pressing temperature, and pressure. The results reveal that the combined effect of temperature and pressure during hot-pressing effectively alleviates the intrinsic long-branched structural constraint of herbaceous lignin, thereby promoting the development of ordered graphite domains during carbonization. Upon optimization of these parameters (stabilization temperature, temperature and pressure during hot-pressing), a highly graphitized carbon material was successfully obtained *via* the hot-pressing process (designated as LSHC-320-290-18). XRD analysis shows a distinct (002) diffraction peak at 25.26°, which represents a significant shift compared to the 23.55° peak of the non-stabilized control (LHC-Raw-250-0). The hot-pressed samples exhibit higher sp²-hybridized carbon content and greater graphitic micro-crystallinity, even at carbonization temperatures lower than those typically required in conventional processing. These results demonstrate that hot-pressing promotes bond reorganization within lignin molecules, establishing favorable conditions for subsequent aromatization and structural adjustments during the carbonization process, thus promoting graphitization.

## 2 Materials and methods

### 2.1 Materials

Enzymatically hydrolyzed lignin from corn-cobs (purity >90%, ash content <1%) was refined and provided by Shandong Longli Biotechnology Co., Ltd. and used as received. Tetrahydrofuran (THF, purity 99.5%) was purchased from Shanghai Acmec

Biochemical Co., Ltd. and used as received. *N,N*-Dimethylformamide (DMF purity 99.5%) and deuterated dimethyl sulfoxide (DMSO, analytical grade) were obtained from Shanghai Mc Calin Biochemical Technology Co., Ltd. and used as received.

### 2.2 Experimental procedure

The raw lignin was initially pulverized using a ball mill (600 rpm, 5 min) to achieve an 80-mesh particle size. Stabilization was subsequently carried out in a muffle furnace at designated temperatures (200, 240, 280, 320, and 360 °C). During stabilization, the temperature was raised from room temperature to 120 °C at a rate of 5 °C min⁻¹, followed by heating to the target temperature at a rate of 1 °C min⁻¹, and maintained 2 h. The resulting stabilized samples were labeled as LS-*x*, where *x* represents the stabilization temperature in °C. After stabilization, 0.4 g of each sample was ground into powder and placed into a custom-designed mold with an area of 1.5 × 1.5 cm for hot-pressing. The hot-pressing process was performed at an initial temperature of 250 °C under a force of 15 tons (equivalent to approximately 666 MPa). The obtained samples were designated as LSH-*x*-250-15. A non-stabilized control (LH-Raw-250-0) was prepared under the same hot-pressing conditions but without applied pressure (0 MPa). Additional hot-pressed samples were prepared by adjusting the hot-pressing temperature and pressures and were labeled as LSH-*x*-*y*-*z*, where *y* represents the hot-pressing temperature and *z* denotes the applied pressure. For carbonization, the LSH-*x*-*y*-*z* and LH-Raw-250-0 samples were placed in crucibles and carbonized in a tube furnace (GSL-1700X, Hefei Kejing Material Technology Co., Ltd) at 1000 °C for 1 h under Ar atmosphere. The resulting carbonized products were labeled as LSHC-*x*-*y*-*z* and LHC-Raw-250-0, respectively.

### 2.3 Characterization

Thermogravimetric analysis (TGA) and differential thermogravimetric analysis (DTG) of lignin were performed using an HTG-1 thermal analyzer (Beijing Hengjiu Instrument Ltd, China). Dried samples were heated from room temperature to 1000 °C under a nitrogen atmosphere at a heating rate of 10 °C min⁻¹. Fourier-transform infrared (FT-IR) spectra were recorded on a Thermo Scientific Nicolet iS10 spectrometer (Thermo Fisher Scientific, Inc., USA) in the range of 750–4000 cm⁻¹. Differential scanning calorimetry (DSC) measurements were conducted using a DSC-BS5 calorimeter (Inno Instruments, Shanghai, China). Approximately 10 mg of sample was placed in the instrument and heated to 350 °C at a rate of 20 °C min⁻¹. The solubility of lignin and lignin-derived samples in tetrahydrofuran (THF) was determined by dissolving 0.2 g of samples in 5 mL of THF and allowing the mixture to stand for 1 h. The insoluble fraction was separated by vacuum filtration, and the solubility was calculated as the mass percentage (%) of the soluble fraction. Solid-state (ss) ¹³C NMR spectra were acquired using a spectrometer from Agilent 600 M, USA. The spectrometer frequency was 150.82 MHz, and the rotating speed was 8000 Hz. X-ray diffraction (XRD) patterns were collected on a Rigaku D/MAX-2500/PC diffractometer equipped with Cu-kα radiation ($\lambda$ = 1.5418 Å) at 40 kV and 70 mA Philips X′ pert

diffractometer. The operating voltage and current were 40 kV and 70 mA, respectively. The $2\theta$ scan range from 5° to 60° at a scanning speed of 0.5° min⁻¹. The interlayer spacing ($d_{002}$) and the corresponding crystallite thickness $L_c$ were calculated according to Bragg's law (1) and Scherrer's eqn (2);

$$d_{002} = \frac{\lambda}{2\sin\theta} \quad (1)$$

$$L_c = \frac{\kappa\lambda}{\beta\cos\theta} \quad (2)$$

In the equations, $\kappa$ is a constant with a value of 0.89, $\lambda$ is the wavelength of the X-ray, $\beta$ is the full width at half maximum (FWHM) of the peak intensity, and $\theta$ is the scattering angle.[22] The surface morphology of the samples was examined by a scanning electron microscope (SEM, TESCAN MIRA4, Shanghai, China) at an acceleration voltage of 5 kV. Raman spectra were recorded using a DXR2xi Raman spectrometer (Thermo Fisher Scientific, Inc., USA) with a 532 nm laser. The D and G band peak areas were fitted using a Gaussian distribution in Origin software. The spectral resolution was approximately 0.5 cm⁻¹. During X-ray photoelectron spectroscopy (XPS) was performed on a Thermo Scientific κ-Alpha (USA) using a monochromatic Al Kα X-ray (1486.6 eV). Transmission electron microscopy (TEM) images were acquired on a FEI Tecnai G2-F20 microscope (USA) at 200 kV. The interlayer spacing was determined using Digital Micrograph software. Pores size distribution and surface area were analyzed via N₂ adsorption/desorption using the Brunauer–Emmett–Teller (BET) on a Sorptomatic 1990 series instrument (Thermo Finnigan, USA).

## 3 Results and discussion

### 3.1 Behavior of lignin at different stabilization temperatures

The chemical structure (FT-IR spectra) and thermal properties (DSC and TGA-DTG curves) of the corncob-derived lignin are presented in Fig. S1. Notably, the lignin exhibits characteristic functional groups, including guaiacyl, syringyl, *p*-hydroxyphenyl, *p*-coumarate, and ferulic acid moieties, which are consistent with typical herbaceous lignin compositions[23] (Table S1). In comparison to hardwood or softwood lignin, herbaceous lignin (from fast-growing species) exhibits elongated side chains and distinct functional groups, as confirmed by 2D-HSQC NMR analysis (Fig. S2, peak assignments in Table S2). This structural configuration, as previously reported,[24] inhibits the formation of aromatic structures during carbonization.

Lignin was first stabilized at different temperatures to obtain samples with different degrees of cross-linking, thereby imparting distinct resistance to deformation during the subsequent hot-pressing step. The extent of cross-linking in the stabilized lignin was compared based on their solubility in THF, as shown in Fig. 1. With increasing stabilization temperature, the color of lignin gradually darkened (Fig. 1a–f). Specifically, the raw lignin exhibited a solubility of 81.1% in THF, while stabilization at 200 °C (designated as LS-200) reduced its solubility to 48.78%. Moreover, Fig. 1g revealed that the solubility of

stabilized lignin underwent a pronounced decline from 9.43% (for LS-240) to 1.00% (for LS-360), a trend that indicated these stabilized samples possessed a notably higher cross-linking degree.

Moreover, Fig. 2 provides additional information on lignin stabilized at different temperatures. It is evident that the stabilization yield decreased from 96.1% (LS-200) to 77.45% (LS-320) and dropped sharply to 66.05% at 360 °C (Fig. 2a). Correspondingly, the glass transition temperature ($T_g$) increased from 189.47 °C (LS-200) to 256.42 °C (LS-320), with the $T_g$ disappearing for LS-360, reflecting the progressive formation of a cross-linked structure at elevated stabilization temperatures (Fig. 2b). Notably, lignin stabilized at elevated temperatures exhibited enhanced thermal stability and a higher residual carbon content at 1000 °C (Fig. 2c and Table S3), with progressive increases in the maximum thermal decomposition temperatures (Fig. 2d). Further insights into the changes in lignin structure were derived from XPS analysis (Fig. 2e). The deconvoluted C 1s spectra (Fig. 2f and Table S4) revealed that the C–O bond content increased from 37.27% in raw lignin to 40.19% in LS-200, whereas the C(O)O groups decreased from 10.75% to 7.77%, which can be attributed to oxidative stabilization in air. In LS-240, C–O bonds began to degrade, with significant reductions observed from LS-280 to LS-360, primarily associated with the cleavage of $\beta$–O–4 bonds, generating phenoxy radicals. Additionally, these phenoxy radicals might have undergone hydroxylation with other oxygen-based radicals, forming phenolic structures. At 320 °C, the C–C bonds also increased dramatically, a trend that continued until 360 °C. Collectively, these observations indicate that 280 °C represents a critical temperature at which lignin molecules cross-linked more rapidly due to C–O bond cleavage and C–C bond formation.

From a chemical perspective, as illustrated in Fig. 2g (FT-IR), lignin stabilized at increased temperatures initially showed an increase in hydroxyl groups up to 200 °C, followed by a subsequent decline. This trend corresponds to the air oxidation of alkyl groups in lignin side chains to form alcoholic hydroxyl groups, which subsequently undergo esterification with carboxyl groups in the system, following the pathway shown in Fig. S3-(1), which is in good agreement with the XPS data. Subsequently, the C–O bond content decreased. This trend indicates the depolymerization of lignin following the pathways outlined in Fig. S3-(2). Furthermore, the formation of interaction between lignin molecules (Fig. S3-(3)) further promoted intermolecular cross-linking.

### 3.2 Behavior of different stabilized lignin upon hot-pressing

The morphological evolution of the hot-pressed samples is shown in Fig. 3. To successfully apply hot-pressing, lignin must be stabilized to form a relatively stable structure to withstand the high pressure applied. Otherwise, lignin (raw lignin and LS-200) immediately experienced powder leakage during hot-pressing (Fig. 3b). On the other hand, if lignin is over-stabilized, it becomes excessively cross-linked and thus difficult to pressurize, resulting in the "non-melting" behavior of the
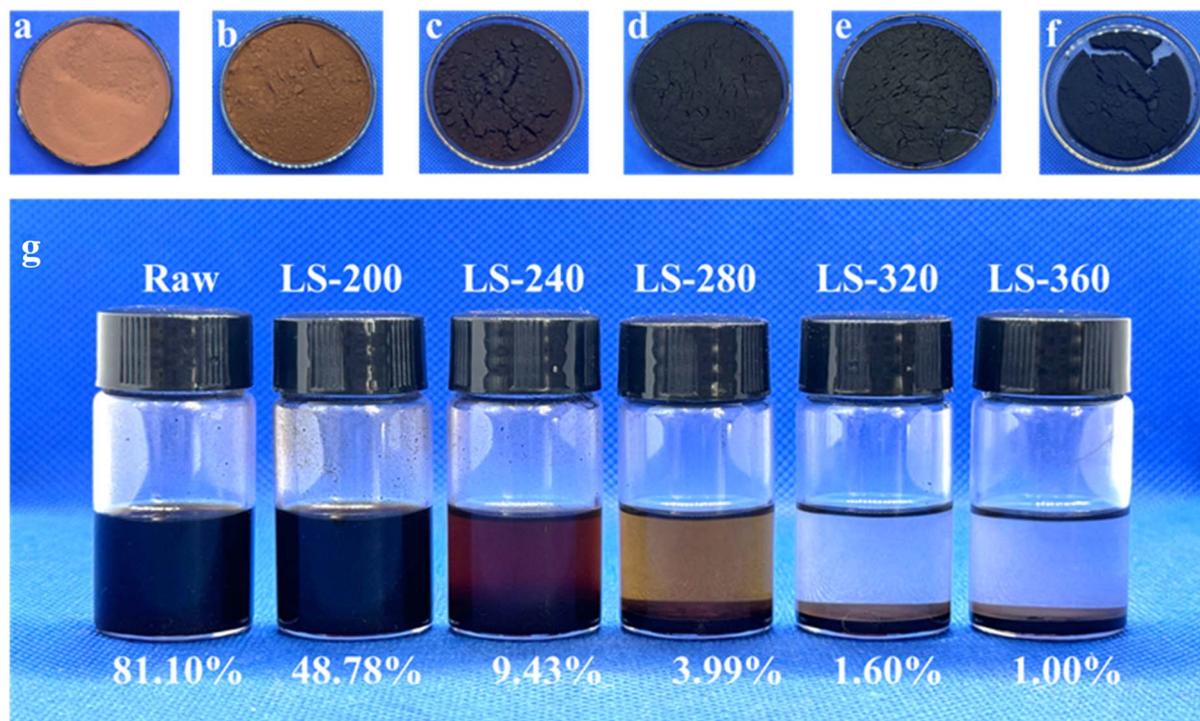
Fig. 1 Appearance evolution of raw lignin and its stabilized derivatives at different stabilization temperatures: (a) raw lignin; (b) LS-200; (c) LS-240; (d) LS-280; (e) LS-320; (f) LS-360; (g) corresponding tetrahydrofuran (THF) solubility test results.

hot-pressed sample (Fig. 3f). The LH-Raw-250-0 exhibited significant volumetric expansion, with a porous architecture clearly visible in the SEM micrographs (Fig. 3a). The LSH-240-250-15 still experienced leakage from the mold but ultimately formed irregular, self-supporting flakes. However, the leakage phenomenon was eliminated in the LSH-280-250-15 and LSH-320-250-15 samples, both of which formed self-supporting flakes (Fig. 3c–e). The progressive thickness increase from 0.57 mm to 0.81 mm confirmed the enhanced compressibility and rigidity of the highly cross-linked lignin, implying that LSH-320-250-15 was more tolerant to high pressure. SEM analysis further revealed that LSH-240-250-15 and LSH-280-250-15 developed dense, cohesive microstructures, while LSH-320-250-15 displayed pronounced surface roughness, which reflects the restricted polymer flow due to advanced cross-linking. The thickness loss rate of lignin before and after hot-pressing at different stabilization temperatures is summarized in Table S5. To highlight the importance of stabilization temperature, the hot-pressing processes of LH-Raw-250-15 and LSH-320-250-15 were compared, as illustrated in Video S1.

The TGA and DTG curves of the hot-pressed samples (including LH-Raw-250-0) are shown in Fig. 4a–c. It can be observed that the lignin stabilized at relatively lower temperatures (200 °C, 240 °C) exhibited a more remarkable increase in $T_{max}$ (i.e., temperature of maximum weight loss rate) after hot-pressing compared with those stabilized at temperatures higher than 280 °C. Additionally, the residual carbon difference before and after hot-pressing showed the same trend as that presented in Fig. 4c. This indicates that lignin stabilized at higher temperatures formed a more cross-linked and stable structure, which is more tolerant to hot-pressing. Especially for LSH-360-250-15, both its $T_{max}$ and residual carbon content remained consistent before and after hot-pressing. The chemical compositions of each sample after hot-pressing are shown in Fig. 4d, e and Table 1. Compared with the stabilized samples before hot-pressing, a relatively large increase in carbon content was observed for LSH-200-250-15, LSH-240-250-15, and LSH-320-250-15. Notably, while LSH-320-250-15 contained the highest proportion of $sp^2$ carbon but the least total carbon in the three samples, indicating that stabilization at 320 °C promotes the formation of $sp^2$ carbon upon hot-pressing. Combined with the morphological data, samples stabilized at 200 and 240 °C were not sufficiently stable to tolerate hot-pressing; thus, more $sp^3$ carbon was formed instead of $sp^2$ carbon. For LSH-360-250-15, although it exhibited the highest carbon content, its $sp^2$ carbon was the least among all hot-pressed samples, indicating that its over-crosslinked structure formed at the high stabilization temperature of 360 °C, thus hot-pressing did not apply effectively.

All hot-pressed samples (including LH-Raw-250-0) were carbonized and subsequently evaluated for their graphitization capabilities. Table S6 summarizes the carbonization yield and overall yield. As a result, the corresponding hot-pressed samples showed different graphitization abilities, and it was found that the samples stabilized at 320 °C and then carbonized exhibited the best performance among all the tested stabilization temperatures (200 °C, 240 °C, 280 °C, 320 °C, 360 °C) by XRD results (Fig. 4f). The 2θ position of (002) peak (indicative of graphitization) was observed at 23.55° for LHC-Raw-250-0, whereas the peak for LSHC-320-250-15 shifted to 24.55°.
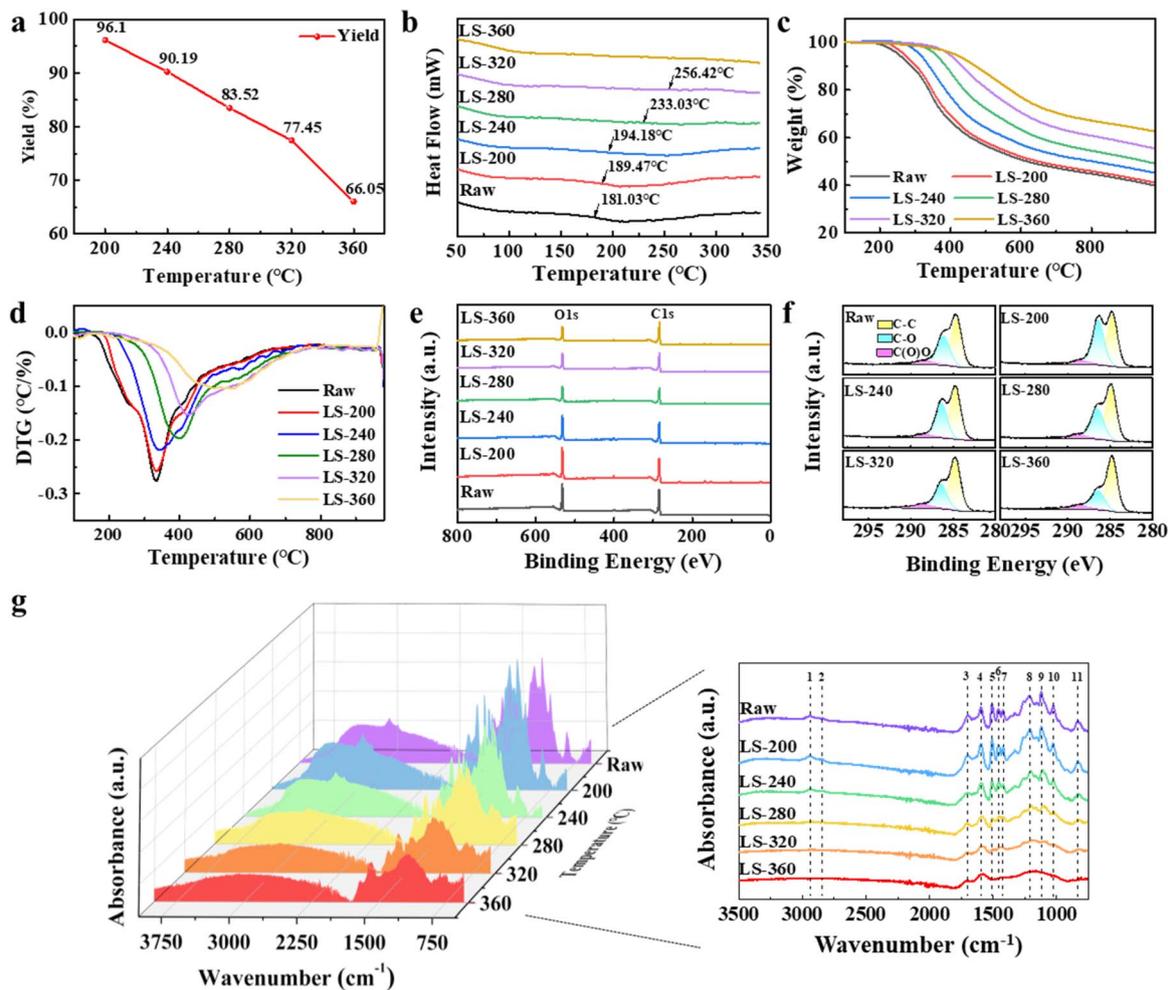
**Fig. 2** Structural and thermal properties of raw lignin and LS–x before hot–pressing: (a) stabilization yield; (b) DSC curves; (c) TGA curves; (d) DTG curves; (e) XPS survey spectra; (f) C 1s spectra; (g) FT-IR spectra.

Notably, the $d_{002}$, which indicates the degree of graphitization (Fig. 4g and Table S7), started to decrease progressively from LSHC-240-250-15 to LSHC-320-250-15, but increased at LSHC-360-250-15 due to excessive cross-linking. These results highlight the existence of an optimal hot-pressing conditions for transforming lignin into a structure favorable for graphitization. The $L_c$ value, representing the lattice thickness of graphite microcrystals, consistently increased from LSHC-240-250-15 to LSHC-360-250-15, implying that higher resistance to hot-pressing is preferable for the formation of thicker lattices, although the effect was modest. It should be mentioned that both lignin stabilized at 280 °C and 320 °C showed good graphitization ability, but lignin stabilized at 320 °C and then upon carbonization exhibited slightly better performance in terms of its position of (002) peak as shown in Table S7, therefore 320 °C was selected as the optimal stabilization temperature for further studies. Although not remarkable, evidence can be found in the subsequent characterization results that indicates 320 °C was the most suitable stabilization temperature to produce hot-pressed lignin with high graphitization ability. According to the Raman spectroscopy results

(Fig. 4h and i), the structure of the material changed significantly after hot-pressing and carbonization. From LSHC-240-250-15 to LSHC-320-250-15, the G-band (associated with the ordered sp$^2$ hybrid carbon vibration in the graphite region) became clearer and stronger, while the D-band (associated with disordered carbon and defects) became weaker. The $I_D/I_G$ ratio decreased from 2.36 to 2.17 (Table S8), indicating a reduced degree of structural disorder. This trend reflects the gradual transformation of amorphous carbon into an ordered graphite structure under appropriate conditions. These observations suggest that suitable stabilization temperature, combined with hot-pressing, enhances the molecular stability of lignin, thereby increasing the yield during subsequent hot-pressing and carbonization steps (Table S9).

A more detailed structural characterization of LH-Raw-250-0 and LSH-320-250-15 (selected for its optimal performance) was performed via solid-state $^{13}C$ NMR (Fig. S4) to elucidate the structural changes induced by the stabilization and hot-pressing (hereinafter referred to as SHP) treatment. Signals below 50 ppm represent alkyl carbons in lignin side chains, which were significantly diminished after SHP. Without SHP
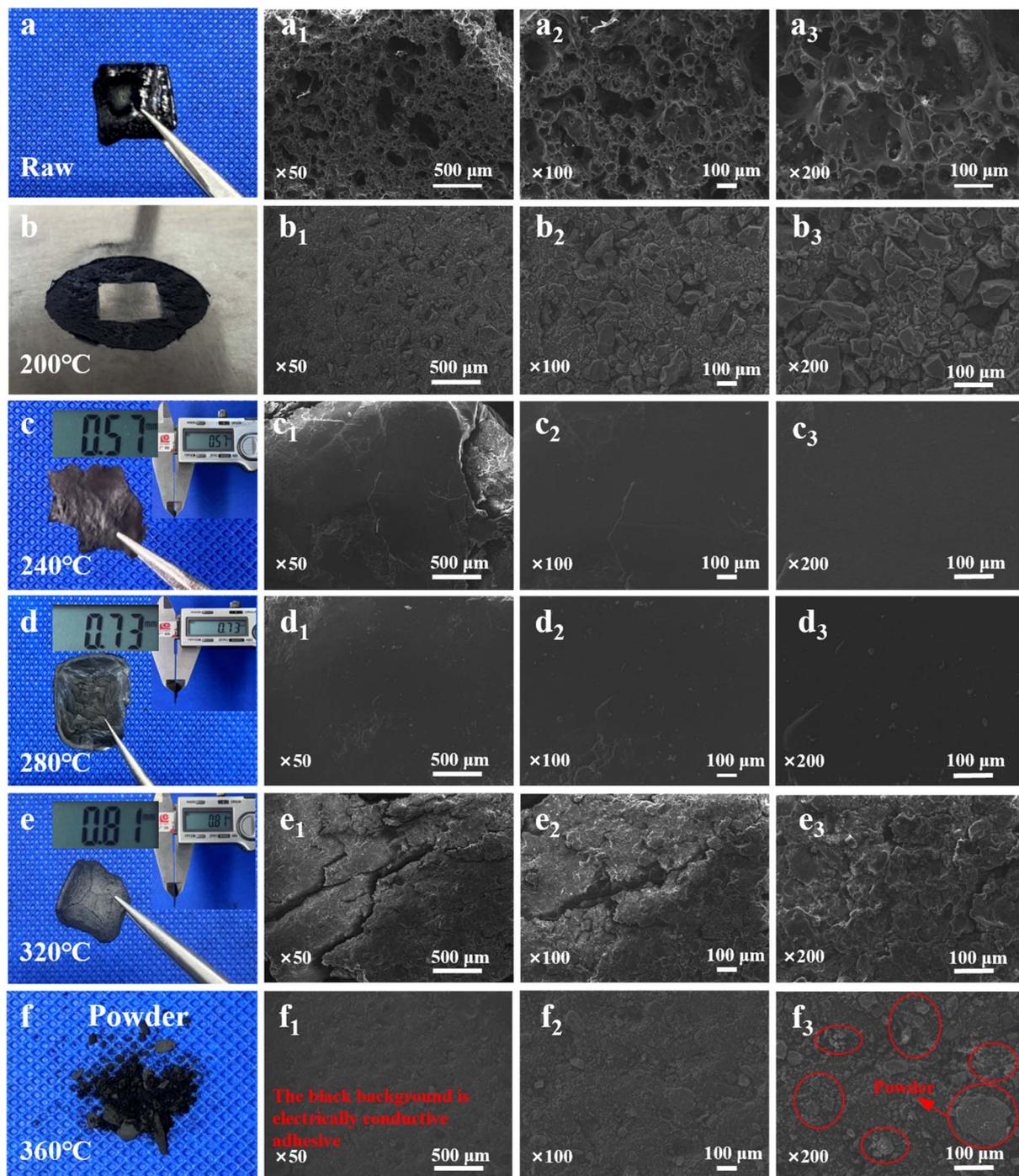
Fig. 3 Morphology and SEM images of (a) LH-Raw-250-0; (b) LSH-200-250-15; (c) LSH-240-250-15; (d) LSH-280-250-15; (e) LSH-320-250-15; (f) LSH-360-250-15.

treatment, lignin exhibited prominent methoxy groups (56–60 ppm),[25] but after SHP, the intensity of these methoxy group signals was markedly reduced. This may have occurred because following SHP treatment, the methoxy groups underwent decomposition by generating radicals on the aromatic ring or dissociating into –O–CH$_3$ radicals at the oxygen atom. Subsequently, these radicals combined with other decomposed compounds, thereby facilitating stable intermolecular

bonding.[9] The carbons on the side chains of LSH-320-250-15, although not distinguishable, showed more varied types compared with those of LH-Raw-250-0, which is also beneficial to the formation of aromatic rings during carbonization. Additionally, broad peaks near 125 and 130 ppm, corresponding to aromatic carbons and molten sp$^2$ carbons, respectively, were significantly stronger in LSH-320-250-15 than in LH-Raw-250-0, confirming that SHP enhanced the formation of
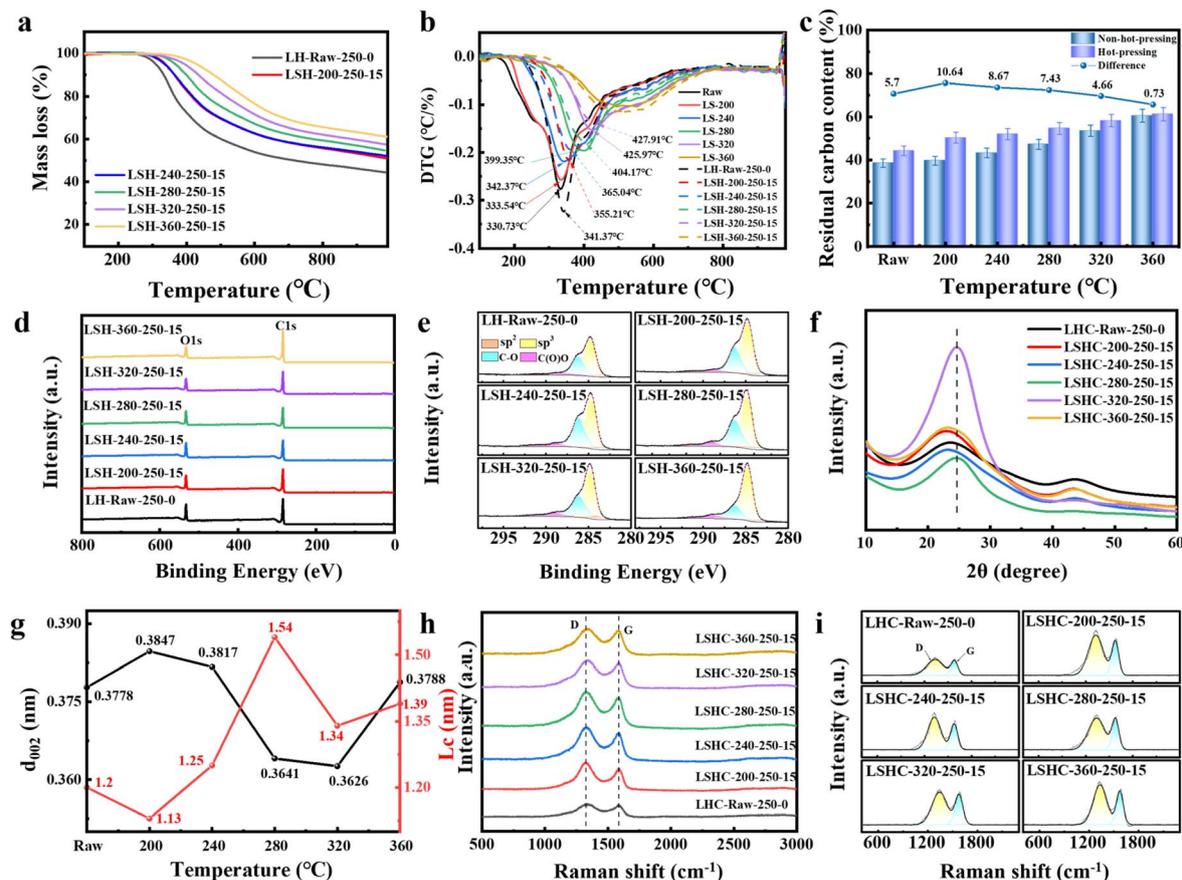
Fig. 4 Characterization of LH-Raw-250-0 and LSH-x-250-15 samples: (a) TGA curves; (b) DTG curves; (c) Residual carbon content comparison before and after hot-pressing; (d) XPS survey spectra, (e) C 1s spectra of the LHC-Raw-250-0 and LSHC-x-250-15 samples characterization; (f) X-ray diffraction profiles; (g) trend diagram of $L_c$ and $d_{002}$; (h) Raman spectra; (i) corresponding Raman fitting results.

aromatic rings. Peaks in the range of 146–190 ppm were associated with aryl C-OR and C-OOR carbons,[27,28] among these, the peak at 148 ppm was primarily attributed to aryl C–O carbon atoms, while the peak at 115 ppm originated mainly from C–H carbon atoms on aromatic rings.[26] These two characteristic peaks were distinctly present in the untreated lignin (LH-Raw-250-0). However, following SHP treatment (LSH-320-250-15), the aryl C–O sites readily participated in condensation and cross-linking reactions, which in turn reduced the content of unstable oxygen-containing functional groups, and this trend is consistent with the reduced intensity of the 146–190 ppm peaks that were observed for the LSH-320-250-15. Similarly, aryl C–H sites also participated in C–C coupling during SHP processing, causing their characteristic peak at 115 ppm to disappear. The

disappearance of the aryl C–O and aryl C–H functional groups enhanced lignin cross-linking and improved structural stability.

### 3.3 Impact of hot-pressing temperature and pressure on the graphitization ability of lignin

Given its optimal performance, LS-320 was selected to systematically evaluate the influence of hot-pressing temperature (230, 250, 270, and 290 °C) on graphitization under a constant pressure of 15 tons. Photographs and SEM images are shown in Fig. S5. With increasing hot-pressing temperature, the sample surface gradually became smoother and the morphology more regular. Under the combined effects of heat and pressure, LS-320 was compacted, with reduced gaps between particles,

Table 1 Proportions of different carbon species in the XPS analysis of lignin samples at different stabilization temperatures after hot-pressing

| Samples | C (%) | O (%) | sp$^2$ carbon (%) | sp$^3$ carbon (%) | C–O (%) | C(O)O (%) |
|---|---|---|---|---|---|---|
| LH-raw-250-0 | 80.44 | 19.56 | 3.14 | 56.30 | 33.22 | 7.34 |
| LSH-200-250-15 | 80.67 | 19.33 | 4.07 | 56.01 | 32.73 | 7.19 |
| LSH-240-250-15 | 78.41 | 21.59 | 4.58 | 49.03 | 38.12 | 8.27 |
| LSH-280-250-15 | 78.44 | 21.56 | 5.48 | 48.89 | 37.00 | 8.63 |
| LSH-320-250-15 | 81.31 | 18.69 | 5.88 | 48.68 | 35.56 | 9.88 |
| LSH-360-250-15 | 83.50 | 16.50 | 3.59 | 62.21 | 25.61 | 8.59 |

resulting in an overall denser structure. Thickness data before and after hot-pressing (Table S10) indicated that higher hot-pressing temperatures resulted in reduced thickness, suggesting that higher temperatures could facilitate the formation of more packed structure under the same pressures. TGA and DTG curves (Fig. 5a and b) of the samples confirmed that while a similar increasing trend was observed with rising hot-pressing temperatures, the effect was not pronounced. FT-IR spectra (Fig. 5d) showed minimal differences in functional groups among the samples. Since the degree of graphitization depends on the proportion of conjugated $sp^2$ carbon atoms, XPS analysis was performed on these samples (Fig. 5e and f), the results showed that the $sp^2$ content increased only slightly, from 4.09% to 7.78% (Table 2). These observations were further corroborated by XRD analysis (Fig. 5g) and Raman spectroscopy (Fig. 5h and i), which indicated no significant differences in the graphitization effect.

This may be attributed to the stabilization temperature (320 °C) had already resulted in a relatively high degree of cross-linking among lignin molecules, thereby limiting further cross-linking during the hot-pressing process. At lower hot-pressing temperatures, it was hard to trigger further reaction of lignin molecules since they had been already well stabilized. Under these conditions, even with a continuous increase in hot-pressing temperature, the applied pressure of 15 tons may still have been insufficient to provide the driving force required to facilitate a higher degree of intermolecular recombination and cross-linking reactions.

To verify this hypothesis, lignin derivatives stabilized at 280 °C were tested under the same hot-pressing conditions as the 320 °C stabilized samples. The results showed that at the lower stabilization temperature, lignin molecules exhibited greater reactivity during hot-pressing, leading to more pronounced structural changes and more significant changes in graphitization effects (Fig. S6 and Table S11).

To enhance graphitization efficiency, the hot-pressing pressure was increased to 18 tons. As the hot-pressing temperature increased, the sample surfaces became progressively smoother and glossier (Fig. S7). XPS analysis (Fig. 6a, b and Table 2) revealed a rapid increase in $sp^2$ carbon content from 7.80% to 17.93%, which is a key factor in enhancing the graphitization of lignin-derived carbons. Additionally, oxygen-containing functional groups (e.g., –C–OR and –COOR) decreased significantly with increasing temperature, reflecting the thermal instability of these functional groups, which had decomposed under the combined effects of temperature and pressure during hot-
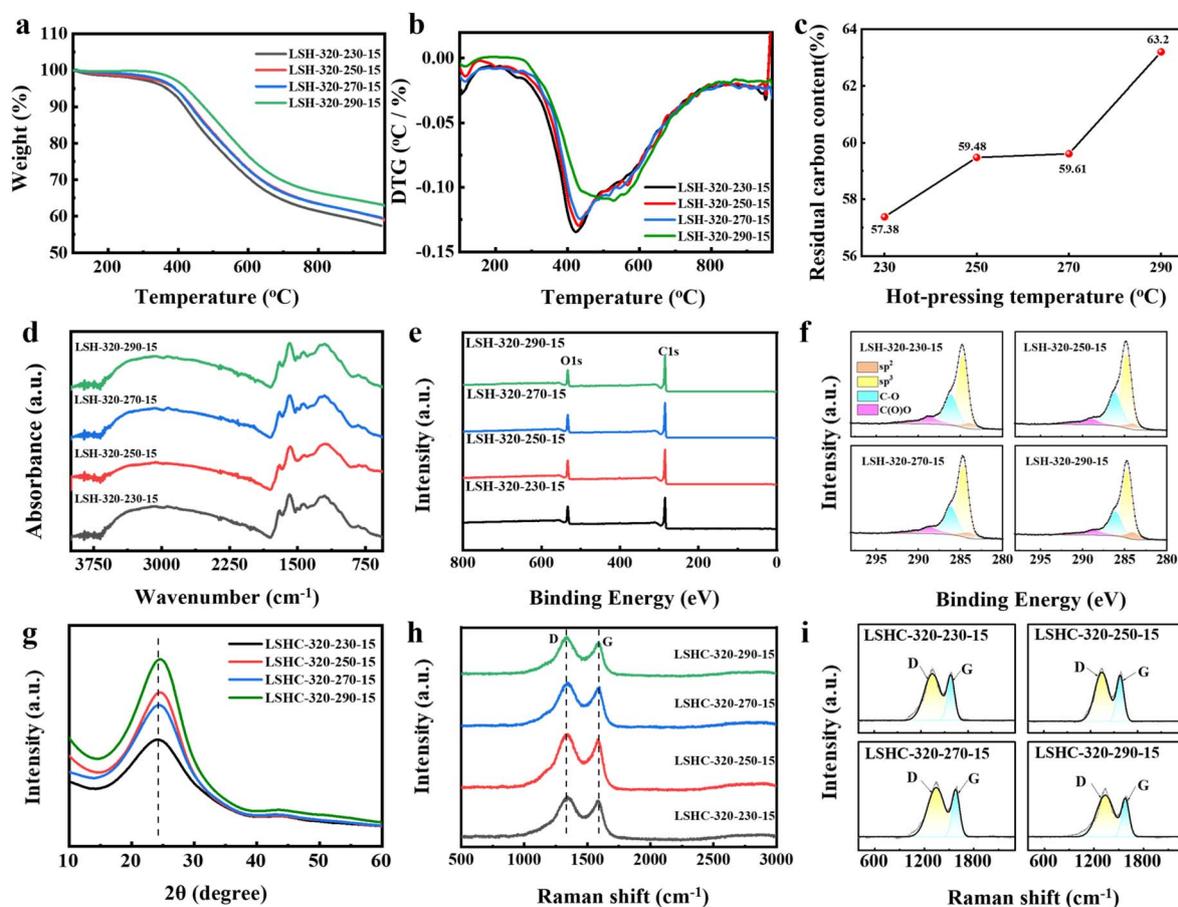


Fig. 5 Characterization of LSH–320–y–15 after treated at different hot-pressing temperatures: (a) TGA curves; (b) DTG curves; (c) residual carbon contents; (d) FT-IR spectra; (e) XPS survey spectra; (f) C 1s spectra; (g) X-ray diffraction profiles; (h) Raman spectra; (i) corresponding Raman fitting result.

**Table 2** Proportions of different carbon species in lignin samples under different hot-pressing conditions by XPS analysis

| Hot-pressing temperature (°C) | Pressures of hot-pressing (t) | C (%) | O (%) | sp² carbon (%) | sp³ carbon (%) | C–O (%) | C(O)O(%) |
|---|---|---|---|---|---|---|---|
| 230 | 15 | 80.25 | 19.75 | 4.09 | 51.13 | 31.58 | 13.20 |
| 250 | 15 | 81.31 | 18.69 | 5.88 | 48.68 | 35.56 | 9.88 |
| 270 | 15 | 81.48 | 18.52 | 6.98 | 53.47 | 29.81 | 9.74 |
| 290 | 15 | 81.04 | 18.96 | 7.78 | 54.29 | 28.27 | 9.66 |
| 230 | 18 | 80.95 | 19.05 | 7.80 | 55.02 | 29.74 | 7.44 |
| 250 | 18 | 80.67 | 19.33 | 11.05 | 54.66 | 27.56 | 6.73 |
| 270 | 18 | 80.76 | 19.24 | 12.94 | 53.95 | 27.02 | 6.09 |
| 290 | 18 | 80.44 | 19.56 | 17.93 | 49.79 | 26.70 | 5.58 |
| 230 | 21 | 80.76 | 19.24 | 6.89 | 52.93 | 32.88 | 7.30 |
| 250 | 21 | 80.77 | 19.23 | 8.64 | 52.52 | 32.13 | 6.71 |
| 270 | 21 | 81.26 | 18.74 | 9.64 | 51.95 | 31.99 | 6.42 |
| 290 | 21 | 81.44 | 18.56 | 13.84 | 49.93 | 30.45 | 5.78 |

pressing. These results confirmed that higher hot-pressing temperature (290 °C) and higher pressure (18 tons) effectively promoted the pyrolysis and polymerization of lignin.

After carbonization of the hot-pressed samples at 1000 °C, the XRD results (Fig. 6c) showed a pronounced (002) peak at 25.26° for the LSHC-320-290-18, indicating enhanced graphitization. The corresponding layer spacing decreased to 0.3525 nm, approaching that of ideal graphite (0.3354 nm). Furthermore, data presented in Table S12 demonstrate that the

crystallite thickness and crystallinity gradually increased with rising hot-pressing temperature, indicating that the pyrolysis and polymerization reaction may have enhanced the degree of cross-linking between lignin molecular chains, thereby promoting improved recombination and more ordered arrangements, and thereby resulting in thicker lattices. Raman spectroscopy results (Fig. S8a, b and Table S13) confirmed these trends. Specifically, compared with the LSH-320-$y$-15 samples, the higher hot-pressing pressure of 18 tons facilitated closer
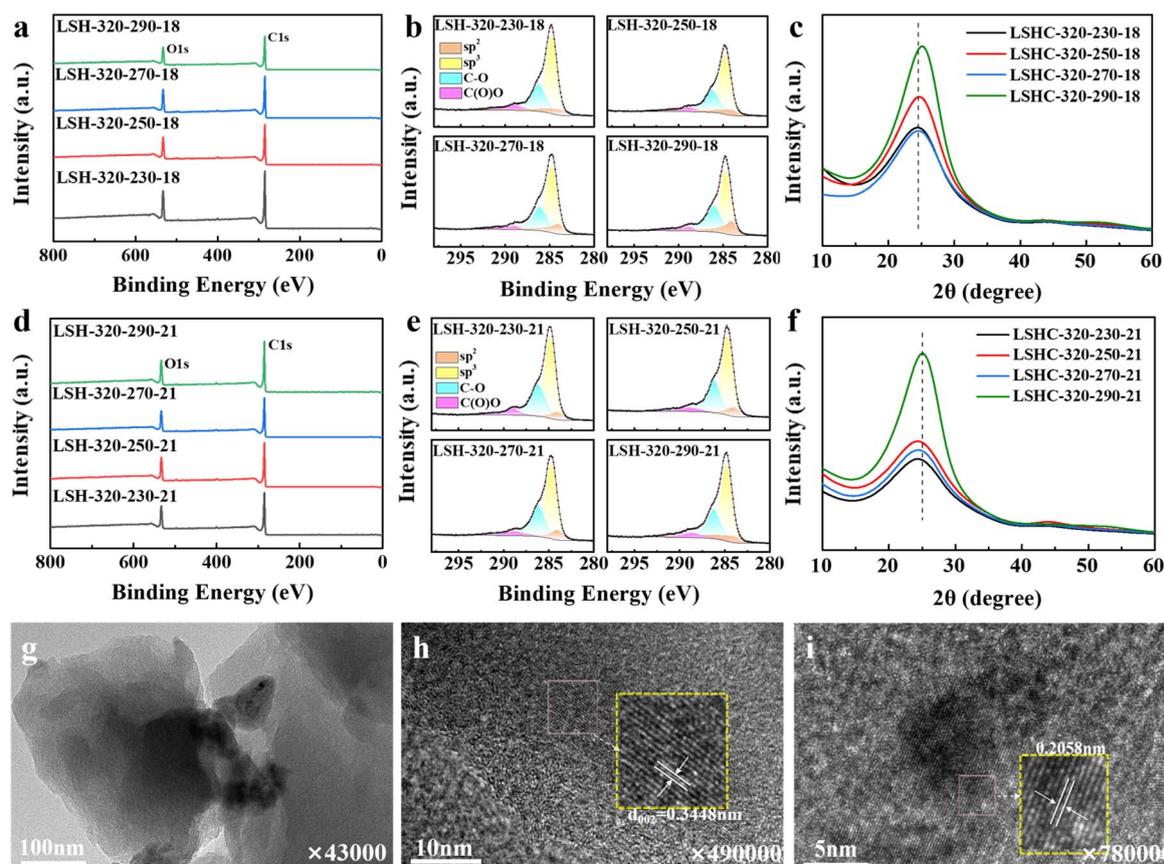


**Fig. 6** (a) XPS survey spectra of LSH–320-$y$-18; (b) C 1s spectra of LSH–320-$y$-18; (c) X-ray diffraction profiles of LSHC–320-$y$-18 samples; (d) XPS survey spectra of LSH–320-$y$-21; (e) C 1s spectra of LSH–320-$y$-21; (f) X-ray diffraction profiles of LSHC–320-$y$-21 samples; (g–i) high resolution TEM (HRTEM) images of LSHC–320-290-18.

intermolecular contact and thereby strengthened intermolecular interactions. Additionally, high temperature and pressure promoted chemical cross-linking reactions, which partially repaired existing structural defects. Consequently, the intensity of the D peak decreased, with the $I_D/I_G$ ratio declining from 2.80 to 2.42, indicating improved carbon ordering.

However, when the pressure was further increased to 21 tons, it was observed (Fig. 6f and Table S12) that the $2\theta$ position of the (002) peak of all corresponding carbonized samples (i.e., LSHC-320-y-21) shifted slightly toward lower angles compared with those obtained under 18 tons (i.e., LSHC-320-y-18), implying that better crystallinity was formed under 18 tons. On the other hand, the $L_c$ values of all LSHC-320-y-18 samples did not show clearly higher values when compared to those of LSHC-320-y-21. XPS data in Table 2 were used to further investigate the differences in chemical bonding between LSHC-320-y-18 and LSHC-320-y-21. As shown in Fig. 6d, e and Table 2, the sp$^2$ carbon ratio in LSHC-320-y-18 samples was consistently higher than that in the corresponding LSHC-320-y-21 samples at all hot-pressing temperatures. Therefore, these results confirmed the presence of a suitable pressure to produce samples with the best graphitization ability under specific stabilization temperatures. The morphological differences of LSH-320-y-18 and LSH-320-y-21 were observed by SEM. As shown in Fig. S7e$_1$–h$_1$, all samples hot-pressed at 21 tons led to the samples with observable cracks (circled with red), and the occurrence of these cracks indicated the merging of lignin molecules could be interrupted if the pressure was excessively high. This may be the reason for the slight reduction of the graphitization ability of the LSH-320-y-21 samples compared with that of LSH-320-y-18 samples.

Compared with non-hot-pressed lignin samples, the hot-pressed samples were more compact. Hot-pressing can enhance the degree of graphitization while affecting the pore characteristics of the materials. As shown in Fig. S9a, the BET surface area of the LSHC-320-290-18 ($S_{BET2} = 122.84$ m$^2$ g$^{-1}$) was much lower than that of the LSC-320 ($S_{BET1} = 205.59$ m$^2$ g$^{-1}$). This phenomenon likely resulted from the partial collapse of pores formed during stabilization due to hot-pressing, leading to a reduction in the number of open pores and a smaller pore diameter. Additionally, lignin molecules were rearranged and cross-linked under hot-pressing, which may have contributed to the partial closure of micropores (<2 nm). High-resolution TEM (HRTEM) images of LSHC-320-290-18 (Fig. 6g–i) revealed an ordered lattice structure with a interlayer spacing of approximately 0.3448 nm, along with observed short-range ordered carbon aggregates. Furthermore, XRD analysis (Fig. S9b) comparing LSC-320 (23.38°) and LSHC-320-290-18 (25.26°) further confirmed that hot-pressing significantly improved graphitization.

## 4 Conclusions

In this study, the graphitization ability of an enzymatically hydrolyzed lignin derived from corn-cobs was systematically investigated by applying stabilized and hot-pressing facilitated carbonization. Results show that the relatively most suitable stabilization temperature for producing graphitizable carbon is 320 °C. At this temperature, the thermal stability of lignin is enhanced and under subsequent hot-pressing the stabilized lignin can be effectively hot-pressed. Upon optimizing the temperatures and pressures of hot-pressing, it was found that 290 °C and 18 tons was the most suitable conditions for further enhancing lignin's graphitization ability. Multiple characterization results have shown that LSH-320-290-18 forms a self-supporting flake with improved structural integrity and higher density, and XPS analysis reveals that the sp$^2$ carbon content in its uncarbonized sample reaches as high as 17.93%. The carbonized LSHC-320-290-18 derivative sample showed a (002) diffraction peak position of 25.26° in XRD analysis, which is notably higher than that of the stabilized and non-hot-pressed sample (LSC-320, 002 peak at 23.38°). HRTEM images also showed the presence of ordered graphitic lattice structure with an interlayer spacing of approximately 0.3448 nm, closing to the 0.3354 nm of graphitic carbon. Overall, this work shows a systematically investigation in terms of stabilization and hot-pressing towards converting a corn-cob derived lignin into graphitizable carbon at only 1000 °C.

## Author contributions

Xiuxia Zhang: conceptualization, data curation, investigation, methodology, writing – original draft, writing – review & editing; Xiao Han: investigation, data curation, methodology; Jing Liu: formal analysis, validation, funding acquisition; Fangxiao Feng: investigation, data curation, methodology; Chen Liang: conceptualization, validation; Linghong Yin: conceptualization, funding acquisition, writing – review & editing; Wangda Qu: conceptualization, methodology, funding acquisition, supervision, writing – review & editing.

## Conflicts of interest

The authors declare that they have no known competing financial interests or personal relationships that could have appeared to influence the work reported in this paper.

## Data availability

The data supporting this article have been included as part of the supplementary information (SI). Supplementary information is available. See DOI: https://doi.org/10.1039/d5ra06833a.

## Acknowledgements

# References

1 X. Ma and G. Zhao, Preparation of carbon fibers from liquefied wood, *Wood Sci. Technol.*, 2010, **44**, 3–11, DOI: 10.1007/s00226-009-0264-3.

2 Y. Long, X. An, H. Zhang, J. Yang, L. Liu, Z. Tian, G. Yang, Z. Cheng, H. Cao and H. Liu, Highly graphitized lignin-derived porous carbon with hierarchical N/O co-doping "core-shell" superstructure supported by metal-organic frameworks for advanced supercapacitor performance, *Chem.–Eng. J.*, 2023, **451**, 138877, DOI: 10.1016/j.cej.2022.138877.

3 C. Chen, K. Sun, C. Huang, M. Yang, M. Fan, A. Wang, G. Zhang, B. Li, J. Jiang and W. Xu, Investigation on the mechanism of structural reconstruction of biochars derived from lignin and cellulose during graphitization under high temperature, *Biochar*, 2023, **5**(1), 51, DOI: 10.1007/s42773-023-00229-7.

4 M. Mennani, A. A. Benhamou, A. A. Mekkaoui, F. El Bachraoui, M. El Achaby, A. Moubarik and Z. Kassab, Probing the evolution in catalytic graphitization of biomass-based materials for enduring energetic applications, *J. Mater. Chem.*, 2024, **12**(12), 6797–6825, DOI: 10.1039/D3TA07449H.

5 F. Torres-Canas, A. Bentaleb, M. Föllmer, J. Roman, W. Neri, I. Ly, A. Derré and P. Poulin, Improved structure and highly conductive lignin-carbon fibers through graphene oxide liquid crystal, *Carbon*, 2020, **163**, 120–127, DOI: 10.1016/j.carbon.2020.02.077.

6 J. S. William, J. Ankush, B. Dylan, A. Salonika, S. Antonio, K. Matthew, P. Seonghyun and S. A. Dimitris, Are lignin-derived carbon fibers graphitic enough?, *Green Chem.*, 2019, **21**, 4253–4265, DOI: 10.1039/c9gc01806a.

7 Q. Yan, J. Li, X. Zhang, E. B. Hassan, C. Wang, J. Zhang and Z. Cai, Catalytic graphitization of kraft lignin to graphene-based structures with four different transitional metals, *J. Nanopart. Res.*, 2018, **20**, 223, DOI: 10.1007/s11051-018-4317-0.

8 M. Yao, X. Bi, Z. Wang, P. Yu, A. Dufresne and C. Jiang, Recent advances in lignin-based carbon materials and their applications: A review, *Int. J. Biol. Macromol.*, 2022, **223**, 980–1014, DOI: 10.1016/j.ijbiomac.2022.11.070.

9 W. Qu, X. Han, J. Liu, L. Yin, C. Liang and P. Hu, Unlocking the graphitization potential of lignin: insights into its transformation through hot pressing and carbonization, *Green Chem.*, 2023, **25**(23), 9873–9883, DOI: 10.1039/D3GC03642A.

10 O. Hosseinaei, D. P. Harper, J. J. Bozell and T. G. Rials, Role of physicochemical structure of organosolv hardwood and herbaceous lignins on carbon fiber performance, *ACS Sustainable Chem. Eng.*, 2016, **4**(10), 5785–5798, DOI: 10.1021/acssuschemeng.6b01828.

11 W. Wang, S. Wang, Y. Pan, X. Ouyang and R. J. Linhardt, Fermented cassava residue lignin prepared by sequential acid steam-explosion and hot-alkaline treatment and its antioxidant properties, *Waste Biomass Valorization*, 2020, **11**, 6115–6124, DOI: 10.1007/s12649-019-00862-z.

12 M. H. Tanis, O. Wallberg, M. Galbe and B. Al-Rudainy, Lignin extraction by using two-step fractionation: a review, *Molecules*, 2023, **29**(1), 98, DOI: 10.3390/molecules29010098.

13 D. Tian, R. P. Chandra, J.-S. Lee, C. Lu and J. N. Saddler, A comparison of various lignin-extraction methods to enhance the accessibility and ease of enzymatic hydrolysis of the cellulosic component of steam-pretreated poplar, *Biotechnol. Biofuels.*, 2017, **10**, 157, DOI: 10.1186/s13068-017-0846-5.

14 H. Yu, W. Xiao, L. Han and G. Huang, Characterization of mechanical pulverization/phosphoric acid pretreatment of corn stover for enzymatic hydrolysis, *Bioresour. Technol.*, 2019, **282**, 69–74, DOI: 10.1016/j.biortech.2019.02.104.

15 Y. Xi, Y. Wang, D. Yang, W. Liu, Q. Li and X. Qiu, $K_2CO_3$ activation enhancing the graphitization of porous lignin carbon derived from enzymatic hydrolysis lignin for high performance lithium-ion storage, *J. Alloys Compd.*, 2019, **785**, 706–714, DOI: 10.1016/j.jallcom.2019.01.039.

16 C. Huang, X. Jiang, X. Shen, J. Hu, W. Tang, X. Wu, A. Ragauskas, H. Jameel, X. Meng and Q. Yong, Lignin-enzyme interaction: A roadblock for efficient enzymatic hydrolysis of lignocellulosics, *Renew. Sustain. Energy Rev.*, 2022, **154**, 111822, DOI: 10.1016/j.rser.2021.111822.

17 J.-K. Lee, J.-G. Kim, K. Hembram, Y.-I. Kim, B.-K. Min, Y. Park, J.-K. Lee, D. J. Moon, W. Lee and S.-G. Lee, The nature of metastable AA'graphite: low dimensional nano- and single-crystalline forms, *Sci. Rep.*, 2016, **6**(1), 39624, DOI: 10.1038/srep39624.

18 S. c. d. Eswaran, S. Subramaniam, U. Sanyal, R. Rallo and X. Zhang, Molecular structural dataset of lignin macromolecule elucidating experimental structural compositions, *Sci. Data*, 2022, **9**(1), 647, DOI: 10.1038/s41597-022-01709-4.

19 A. Kirui, W. Zhao, F. Deligey, H. Yang, X. Kang, F. Mentink-Vigier and T. Wang, Carbohydrate-aromatic interface and molecular architecture of lignocellulose, *Nat. Commun.*, 2022, **13**(1), 538, DOI: 10.1038/s41467-022-28165-3.

20 D.-L. Li, J.-Q. Wu, W.-X. Peng, W.-F. Xiao, J.-G. Wu, J.-Y. Zhuo, T.-Q. Yuan and R.-C. Sun, Effect of lignin on bamboo biomass self-bonding during hot-pressing: lignin structure and characterization, *BioResources*, 2015, **10**(4), 6769–6782.

21 P. K. Karoki, S. Zhang, Y. Pu and A. J. Ragauskas, Lignin-based vitrimers: valorization and utilization of lignin in high-value applications, *Mater. Adv.*, 2024, **5**, 7075–7096, DOI: 10.1039/D4MA00281D.

22 T. Qiu, J.-G. Yang, X.-J. Bai and Y.-L. Wang, The preparation of synthetic graphite materials with hierarchical pores from lignite by one-step impregnation and their characterization as dye absorbents, *RSC Adv.*, 2019, **9**, 12737–12746, DOI: 10.1039/C9RA00343F.

23 G. Wang and H. Chen, Fractionation of alkali-extracted lignin from steam-exploded stalk by gradient acid precipitation, *Sep. Purif. Technol.*, 2013, **105**, 98–105, DOI: 10.1016/j.seppur.2012.12.009.

24 Y. Wang, W. Liu, L. Zhang and Q. Hou, Characterization and comparison of lignin derived from corncob residues to better understand its potential applications, *Int. J. Biol. Macromol.*, 2019, **134**, 20–27, DOI: 10.1016/j.ijbiomac.2019.05.013.

25 X. Zhang, Q. Yan, W. Leng, J. Li, J. Zhang, Z. Cai and E. B. Hassan, Carbon nanostructure of kraft lignin thermally treated at 500 to 1000 °C, *Materials*, 2017, **10**(8), 975, DOI: 10.3390/ma10080975.

26 S. Ueno, E. Mizushima, N. Chatani and F. Kakiuchi, Direct observation of the oxidative addition of the aryl carbon-oxygen bond to a ruthenium complex and consideration of the relative reactivity between aryl carbon-oxygen and aryl carbon-hydrogen bonds, *J. Am. Chem. Soc.*, 2006, **128**(51), 16516–16517, DOI: 10.1021/ja067612p.

27 Q. Zheng, D. Zhang, P. Fu, A. Wang, Y. Sun, Z. Li and Q. Fan, Insight into the fast pyrolysis of lignin: Unraveling the role of volatile evolving and char structural evolution, *Chem.–Eng. J.*, 2022, **437**, 135316, DOI: 10.1016/j.cej.2022.135316.

28 J. Braun, K. Holtman and J. Kadla, Lignin-based carbon fibers: Oxidative thermostabilization of kraft lignin, *Carbon*, 2005, **43**(2), 385–394, DOI: 10.1016/j.carbon.2004.09.027.